

1 Seasonal sediment dynamics on the Barcelona inner shelf (NW Mediterranean):
2 A small Mediterranean river- and wave-dominated system

3 L. López^{a,*}, J. Guillén^a, A. Palanques^a, M. Grifoll^b

4 ^a Department of Marine Geosciences, Institut de Ciències del Mar (CSIC), Passeig Marítim de la Barceloneta 37–49, 08003,
5 Barcelona, Spain

6 ^b Department of Civil and Environmental Engineering, BarcelonaTech (UPC), c./Jordi Girona, 1–3, 08034 Barcelona, Spain

7 **Abstract**

8 The seasonal pattern of sediment dynamics on an inner shelf characterized by the presence
9 of sediment delivered by a small, mountainous river (with a “flash-flood” regime) was
10 investigated. Near-bottom suspended sediment fluxes across the shelf (i.e. 20, 30 and 40 m
11 water depth) were estimated using observations from three benthic tripods deployed from
12 September 2007 to June 2008. Near-bottom sediment resuspension is controlled by wave-
13 induced currents and river-born sediment availability, whereas the shelf currents play a
14 secondary role. Fourteen sediment transport events were identified (eight in autumn, two in
15 winter and four in spring), with transport rates according to storm intensity and sediment
16 availability. These few energetic events induced a large percentage of the cumulative
17 sediment transport near the bottom. However, the lack of proportionality between suspended
18 sediment transport rates and the combined wave-current bottom shear stress in some events
19 highlights the importance of the sequence of events in sediment dynamics. Since wave
20 activity, hydrography and river discharges display a strong seasonal pattern in the NW
21 Mediterranean, the resulting sediment dynamics across the shelf also correspond to a
22 seasonal cycle. This seasonal variability leads to a temporal evolution of the bottom grain
23 size (coarser in winter) and the near-bottom sediment transport rates (higher in spring and
24 autumn) which is consistent with the seasonal pattern of the hydrodynamic events and the
25 river discharge load.

26 *Keywords: Sediment resuspension; sediment transport events; river-born sediment availability; flash-*
27 *flood regime; mountainous river; Besòs River.*

* Corresponding author. Tel.: +34 932 309 600; Fax: +34 932 309 555. E-mail: (L.López).

28 **1. Introduction**

29 The influence of river floods and storms on sediment delivery and reworking has been
30 recognized in many recent studies of river-dominated continental shelves, where river inputs
31 and storm waves have been found to be the dominant forcing mechanisms of sediment
32 dynamics (e.g. Cacchione et al., 1995; Ogston and Stenberg, 1999; Sherwood et al., 1994).
33 In small-river systems (drainage basins $<10^4$ km²), where most of the annual sediment load
34 is discharged during episodic events, the short duration of floods can lead synoptic-scale
35 (days to weeks) meteorological forcing to have a more important role in the fate of the
36 sediment discharged onto the continental shelf (Bever et al., 2011; Geyer et al., 2000).
37 Discharged sediment from small-river floods can remain close to the river mouth on shelves
38 with micro-tidal conditions and moderate significant wave heights. In these cases, sediments
39 that are deposited nearshore can be subsequently resuspended and transported to distal
40 portions of the system when shear stresses become sufficiently high (Grifoll et al., 2014;
41 Guillén et al., 2006). The suspended load is then the main sediment transport mechanism
42 resulting in sediment winnowing and erosion across the shelf (Allison et al. 2000; Grifoll et
43 al., 2013_1).

44 The NW Mediterranean Sea is a micro-tidal and low-energy system from the wave climate
45 perspective. Floods and storm-generated wave effects on coastal sediment resuspension
46 and transport on the shelf have been emphasized by several studies on the Ebro continental
47 shelf (Guillén et al., 2002; Jiménez et al., 1999; Palanques et al., 2002; Puig et al., 2001) and
48 on other shelves of the northwestern Mediterranean (Dufois et al., 2014; Ferré et al., 2005;
49 Guillén et al., 2006; Palanques et al., 2011; Roussiez et al., 2005; Ulses et al., 2008). These
50 investigations revealed that wave-induced bottom shear stress is generally the main stirring
51 factor for sediment resuspension and transport and is mainly effective in the inner shelf
52 region. However, strong storm waves could also resuspend fine-grained sediments from the
53 mid-shelf and transport them off-shelf (Puig et al., 2001; Simarro et al., 2015). The along-
54 shelf sediment fluxes are dominant during most of the time on NW Mediterranean continental
55 shelves (Grifoll et al., 2013_1; Palanques et al., 2002), although it has been reported that
56 extreme floods and storms in the Gulf of Lions can lead to across- and along-shelf sediment
57 transport of about the same order of magnitude (Bourrin et al., 2008; Palanques et al., 2011;
58 Ulses et al., 2008). The resulting surface sediment distribution and the location of the
59 prodeltaic mud deposits have been observed to be coherent with the hydrodynamic
60 processes and induced near-bottom sediment fluxes. The finest sediment accumulates
61 mainly on the mid-shelf, where the lowest mean combined wave-current shear stresses
62 occur, whereas on the inner shelf some mud accumulates but is frequently resuspended due

63 to the high combined wave-current shear stresses occurring in this region (Grifoll et al., 2014;
64 Palanques et al., 2002).

65 As yet, few studies have addressed sediment dynamics on continental shelves off a “small”
66 Mediterranean river system (e.g. the Têt River in the Gulf of Lions: Bourrin et al., 2008;
67 Guillén et al., 2006). Guillén et al. (2006) differentiated episodes of sediment dispersal on the
68 inner shelf of the Têt River during “wet storms”, when storm conditions coincide with local
69 precipitation and elevated river discharge, and “dry storms”, when storm waves occur in the
70 absence of significant river discharge. [The main differences between the wet and dry storms](#)
71 [arose after the storm. This “small” Mediterranean river system allows the deposition of fine-](#)
72 [grained particulate material near the river mouth during flood events as ephemeral layers.](#)
73 [Their location above the storm wave base make them subjected to regular resuspension](#)
74 [events that transport these fine materials further offshore.](#) Further, Bourrin et al. (2008)
75 analysed sediment dynamics from a flood event with a five-year return interval in the Têt
76 River basin and on the adjacent inner shelf of the Gulf of Lions. [Their results show that floods](#)
77 [with a few-year return interval in small coastal rivers can play a significant role in the](#)
78 [transport of sediments on microtidal continental margins and their export from the shelf](#)
79 [through canyons.](#) However, no study has been published on seasonal characterization of
80 sediment dynamics in a “small” Mediterranean river system.

81 [The present study investigates sediment dynamics in the shelf and quantifies sediment](#)
82 [transport on a micro-tidal inner shelf influenced by a small Mediterranean river, the Besòs](#)
83 [River \(Barcelona, NW Mediterranean Sea – Figure 1\). In particular, this study focuses on the](#)
84 [effect of floods and storms on sediment dynamics over a year, emphasizing in the](#)
85 [characteristics of the forcing conditions during sediment transport events and their frequency](#)
86 [and distribution along the seasons of the year \(i.e. the seasonal variability of near-bottom](#)
87 [sediment transport\).](#)

88 The paper is organized as follows. Section 2 introduces the study area characteristics and
89 the methods used to obtain the data analysed thereafter. Section 3 includes the analysis of
90 the meteo-oceanographic forcing conditions and the momentum terms in both along- and
91 across-shelf directions; we examine the seasonal variation at a point where water velocity
92 data are available (near-bottom at 20, 30 and 40 m water depth) and the variability of the
93 bottom sediment grain size and seabed level in response to these meteo-oceanographic
94 conditions throughout the study period. Section 4 considers the representativeness of the
95 results, and in particular the way in which sediment dynamics respond to different forcing

96 mechanisms and the role played by stratification. Finally, in Section 5, we present some
97 conclusions on the seasonal sediment dynamics patterns off a small Mediterranean river
98 system obtained from the analysis in Section 4.

99 **2. Methods**

100 **Study area**

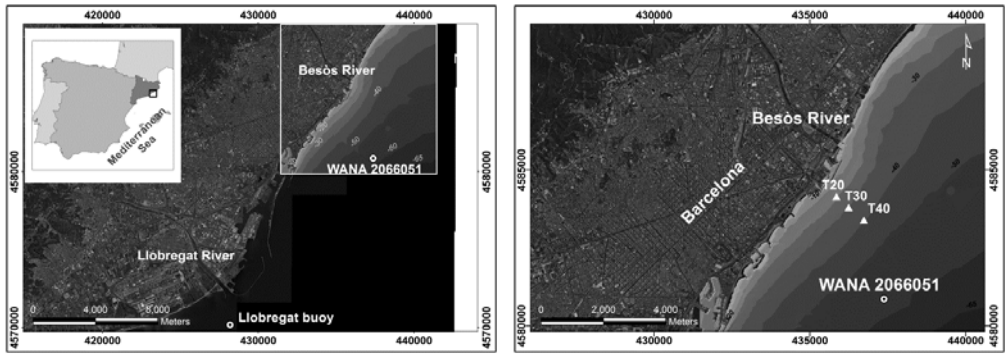
101 The Besòs River is a short river with a mountainous basin of 1029 km² and its main course
102 flows north-south along 52 km from the Catalan Coastal Ranges to the Mediterranean Sea.
103 Its water discharge is variable, with higher values in spring and autumn and minimum values
104 in summer (Liquete et al., 2009; Palanques and Díaz, 1993). Mean water discharge between
105 1968 and 2008 was 6.8 m³/s at the gauging station located 2.8 km upstream from the river
106 mouth, where the maximum water discharge of 270 m³/s was measured on 9 May 1991
107 (Liquete et al., 2009). The sediment load in the lower part of this river is affected seasonally
108 by relatively intense rains (Palanques, 1994). [The sandy sediment developed a small delta
109 plain and the fine sediment developed the prodelta \(Checa et al., 1988\)](#). The Besòs River
110 annual sediment discharge, averaging 15000 t/year, forms a delta of 8.3 km² with a coastal
111 development of 7.6 km shifted southwestwards from the river mouth as a result of the
112 dominant littoral circulation (Liquete et al., 2007).

113 Statistical analysis of wave conditions in the region from 1984 to 2004 showed a mean
114 significant wave height value (Hs) of 0.70 m, an Hs maximum of 4.61, a maximum wave
115 height of 7.80 m and an averaged mean period of 4.29 s (Gómez et al., 2005). Storms occur
116 mainly from October to April and the most important ones are those coming from the east,
117 due to the combination of the coastal orientation and the Mediterranean climate (Bolaños et
118 al., 2008; Sánchez-Arcilla et al., 2008). The winds are characterized by little inter-annual
119 variability (Cerralbo et al., 2015; Font, 1990). The predominant winds come primarily in
120 autumn and winter from the north and northwest, where their energy is concentrated in low
121 frequencies associated with low-pressure systems, which in this area of the NW
122 Mediterranean Sea corresponds to 3-12 days. In summer and spring, the dominant winds are
123 southwesterly, with the dominant frequencies being the low-pressure systems and diurnal
124 (sea breeze) bands (Cerralbo et al., 2015; Font, 1990). On the inner part of the shelf, the
125 frictional forces tend to prevail, leading to a predominance of depth-averaged along-shelf
126 flows over depth-averaged across-shelf flows; the depth-averaged along-shelf flow variability
127 is driven basically by local wind-forcing and remote sea level gradients, and is influenced by
128 water column stratification and rapid pulses of river discharge (Grifoll et al., 2012; 2013_2).
129 The tidal range is lower than 0.2 m.

130 The Barcelona continental shelf is a narrow shelf (6–20 km) with the shelf break at 110–120
131 m depth (ITGE, 1989). The Llobregat and Besòs Rivers provide the main sediment supply,

132 which tends to be transported southwestward due to the action of the dominant along-shelf
 133 current (Flexas et al., 2002; Font et al., 1995; Rubio et al., 2005). The monitoring of sediment
 134 dynamics in the coastal zone of Barcelona reveals frequent resuspension of bottom sediment
 135 caused by waves during storms (Antonijuan et al., 2012; Grifoll et al., 2013_1), and only the
 136 finest fractions can be transferred to the slope and beyond through permanent nepheloid
 137 layers (Palanques et al., 2008; Puig and Palanques, 1998). The sediment distribution
 138 therefore has the same characteristics as other Mediterranean shelves that receive
 139 significant discharges from rivers (Liquete et al., 2010; Palanques et al 1990; Palanques and
 140 Díaz, 1994; Puig et al., 1999): (1) medium- to well-sorted sand (0.25 mm) in less than 15 to
 141 20 m water depth; (2) mostly silt and clay (0.0078 to 0.0039 mm) distributed to the south
 142 from the mouth of the Besòs River between 20 and 60 m depth; and (3) biogenic relict silty
 143 sand (0.0625 to 0.125 mm), which covers the shelf from 60 m depth to the continental slope.
 144 Liquete et al. (2007) recognized two main morphosedimentary domains: a modern, river-
 145 influenced area and a relict, sediment-depleted area. The modern, river-influenced shelf
 146 includes the Llobregat and Besòs adjacent prodeltas, which represent the main Holocene
 147 depocenter in the area located between 30 and 60 m water depth.

148



149

150 *Figure 1. Maps of the Barcelona continental shelf showing the study area and the position of the benthic tripods*
 151 *deployed: T20 at 20 m water depth, T30 at 30 m depth and T40 at 40 m depth. The map projection is UTM zone*
 152 *31N datum ED50.*

153 **Data collection**

154 Three benthic tripods were deployed on the Barcelona continental shelf at 20, 30 and 40 m
 155 water depths (Figure 1) during the four SEDMET field cruises carried out from September
 156 2007 to June 2008 aboard the R/V *García del Cid* and the R/V *Sarmiento de Gamboa*. Each
 157 tripod was equipped with several sensors and instruments: an Aanderaa Doppler current
 158 meter (RCM-9) coupled with a pressure sensor and an Aanderaa optical backscatter

Formatat: anglès (EUA)

Comentari [LL1]: Es demasiado pequeña?
 No se apreciaba todo en una figura y he hecho dos y como mejor quedan es de lado pero quizás es muy pequeña!!

159 turbidimeter placed at 0.53 metres above bottom (mab) and a NKE ALTUS altimeter placed
160 at 0.22 mab. In addition, a set of vertical hydrographic profiles, surficial and near-bottom
161 water samples and bottom sediment samples were obtained along the tripod transect during
162 the deployments. The hydrographic profiles were made using a Sea-Bird SBE 9 CTD
163 coupled with a Seapoint turbidimeter and a set of Niskin bottles. Data collection was carried
164 out in one day in order to obtain a quasi-simultaneous picture of the hydrographic and
165 nepheloid structures. Sediment samples were collected with a small box corer with one
166 acrylic cylindrical core tube (inner diameter = 135 mm) designed to obtain an undisturbed
167 sediment core with a maximum length of 30 cm.

168 The first deployment was carried out at the beginning of autumn (27–29 September 2007) to
169 define the initial conditions of the system in terms of hydrography and bottom sediment
170 characteristics. The second and third deployments (28–30 November 2007 and 28–29
171 February 2008, respectively) were scheduled to perform equipment maintenance tasks and
172 to collect representative samples of the bottom sediment and the hydrographic structure of
173 autumn and winter, respectively. Finally, on 19 June 2008 the equipment was recovered and
174 the bottom sediment sampling and hydrographic profiles were performed to characterize the
175 area at the end of the spring season, which corresponded to the end of the study period. The
176 field data recovered in each deployment are listed in Table 1.

FIELD DATA		SEDMET-I (27/09/07)	SEDMET-II (28/11/07)	SEDMET-III (28/02/08)	SEDMET-IV (19/06/08)	
HYDROGRAPHY	Hydrographic Profiles	3	3	3	3	
SEDIMENT SAMPLES	Sediment Cores	3	3	3	3	
TRIPODS	T20	DEPLOYMENT	Current Velocity	Ok	Ok	Ok
			Pressure	Ok	Ok	Ok
			Turbidity (0-20 NTU range)	Ok	Ok	Ok
			Seabed Level	Failed	Partly	Ok
	T30		Current Velocity	Ok	Ok	Partly
			Pressure	Ok	Ok	Partly
			Turbidity (0-20 NTU range)	Ok	Ok	Partly
			Seabed Level	Failed	Partly	Ok
	T40		Current Velocity	Ok	Not recovered	Not recovered
			Pressure	Ok		
			Turbidity (0-20 NTU range)	Ok		
			Seabed Level	Failed		

177 *Table 1. Available field data summary during the study period.*

178 Wave measurements from the Llobregat directional buoy were used as wave conditions
179 during the study period. This buoy was located at 45 m water depth (Figure 1) and recorded
180 data every hour. Interruptions in the buoy time series were filled in with data from the WANA
181 model (50 m water depth, Figure 1), which provides directional wave information every three
182 hours. The WANA data have been computed by the Spanish National Institute of
183 Meteorology using the HIRLAM and WAM numerical model since 1991 (Spanish Port
184 Authority). Wave height and period data from the WANA model were calibrated through
185 linear regression using the buoy observations from October 2001 to December 2008
186 (Sancho-García et al., 2013). [Winds were also obtained from the WANA data set and rotated](#)
187 [following the orientation of the isobaths \(42°\) to obtain the across and along components.](#)
188 The Besòs River daily discharge was obtained from the Catalan Water Agency water
189 discharge gauging station located 2.8 km upstream from the Besòs River mouth.

190 **Data processing**

191 [Shallow-water effects in the swell: The shoaling and refraction coefficients were calculated to](#)
192 [correct wave height as waves move from the 45 m depth \(buoy location\) to the 20 m, 30 m](#)
193 [and 40 m sites, where the instruments were deployed. The shoaling \(\$k_s\$ \) and refraction \(\$k_r\$ \)](#)
194 [coefficients were approximated with a MATLAB function following the manual computation](#)
195 [methods taken from WMO \(1998\):](#)

$$k_s = \frac{H}{H_0} = \sqrt{\frac{C_{g0}}{C_g}} = \sqrt{\frac{1}{2} \frac{C_0}{C_g}}$$

196 where C_0 is the phase velocity in deep water ($\sqrt{g/k_0}$), k_0 is the wavenumber in deep water
 197 and H_0 is the wave height in deep water.

$$k_r = \frac{H}{H_0} = \sqrt{\frac{\cos \alpha_0}{\cos \alpha}}$$

198 where α_0 is the angle between a wave crest and a local isobath in deep water.

199 Shear velocities and the total maximum shear stress: A one-dimensional (1D) sediment
 200 transport model (Harris and Wiberg, 1997; 2002; Wiberg and Smith, 1983; Wiberg et al.,
 201 1994) was used to predict the wave and current near-bottom velocity profiles, values of
 202 boundary shear stress and compute suspended sediment concentration, which presented
 203 good agreement with the observational data during times of elevated wave shear velocity
 204 (data not shown).The model represented the frictional momentum balance in the bottom
 205 boundary layer using an eddy viscosity profile enhanced by wave-current interaction. Then,
 206 the total shear stress is computed in such a way as to account for differences in direction
 207 between the waves and the current:

$$\tau_{cw} = [(\tau_{cp} + \tau_w)^2 + \tau_{cn}^2]^{1/2}; \tau_w = \rho U_{*w}^2, \tau_{cp} = \rho U_{*c}^2 \cos \varphi, \tau_{cn} = \rho U_{*c}^2 \sin \varphi$$

208 where, τ_w is the boundary shear stress associated with the waves, τ_{cp} and τ_{cn} are the wave-
 209 parallel and wave-normal components of the mean current boundary shear stress,
 210 respectively; ρ is the water density; U_{*c} and U_{*w} are the shear velocities for the current and
 211 waves, respectively; and φ is the difference in the direction of the waves and the current.

212 The time series of current velocities measured at 0.53 cm above bottom, wave period and
 213 direction and the near-bottom wave-orbital velocity were used as inputs to the model, along
 214 with the bed characteristics: the average measured bed sediment size distribution, bed
 215 sediment concentration (1 – porosity) and the resuspension parameter (γ_0), based on grain-
 216 size and geotechnical analysis. The sediment size distribution represents 6 sediment
 217 fractions for the upper centimetre at each location and for each deployment with the
 218 corresponding critical shear stress for initiation of motion and settling velocity, estimated
 219 using the methodology of Soulsby (1997). The bottom wave-orbital velocity was calculated
 220 using the method implemented by Wiberg and Sherwood (2008), which consist in a MATLAB

221 [function for calculating the representative bottom orbital velocity \(\$U_{br}\$ \) from \$H_s\$ and \$T_p\$ using a](#)
222 [parametric spectrum.](#)

223 [Calibration of turbidimeters and grain size analysis:](#) Turbidimeters express the light scattering
224 intensity as an equivalent of Formazin turbidity Units (FTU). This calibration was conducted
225 by the manufacturer using Formazin (turbidity calibration standards). In order to convert FTU
226 units into concentration units (mg/L), turbidity sensors were transformed using the
227 measurements obtained by Guillén et al. (2000) from 25 northwestern Mediterranean
228 samples taken in a nearby area. The intensity of the light backscattered by particles was
229 calibrated with a Formazin solution to calculate the suspended sediment concentration (SSC)
230 with the equation:

$$SSC(mg/L) = 1.21FTU + 0.43 \quad (r^2 = 0.46)$$

231
232 The sediment grain size distribution from the sediment samples was determined by a settling
233 tube for the fraction $>50 \mu m$ and by a Sedigraph 5100D (Micrometrics) for the fraction <50
234 μm following the method described by Giró and Maldonado (1985).

235 [Along- and across-shelf currents and near-bottom suspended sediment fluxes: Aanderaa](#)
236 [current meters \(0.58 mab\) output the module of the current intensity and direction measured](#)
237 [from the north. These were decomposed to u and v components with positive values towards](#)
238 [the N and E, respectively. The along- and across-shelf components were then defined](#)
239 [following the orientation of the isobaths \(\$42^\circ\$ for all sites\), with positive values towards the NE](#)
240 [and offshore, respectively. Assuming that the output of the backscatter sensors was largely](#)
241 [attributable to suspended particles and that particles move with the velocity of the water](#)
242 [within which they are suspended \(Wright, 1995\), the instantaneous near-bottom sediment](#)
243 [flux \$q\$ in \$g/m^2s\$ at the height of the instrument is obtained as the product of the velocity](#)
244 [module \$c\$ and the SSC, in mg/L:](#)

$$q(t) = c(t)SSC(t)$$

245 [Averaging sediment flux over time produces the estimated magnitude of the advective flux](#)
246 [and its direction from each sampling site during the experiment. The along-shelf and across-](#)
247 [shelf advective sediment flux components were obtained in the same manner as the product](#)
248 [of the SSC and the along and across components of the velocity fields. From the resulting](#)

249 [vector \(magnitude and direction\) of the along and across-shelf suspended flux we can obtain](#)
250 [the horizontal net flux for a selected interval.](#)

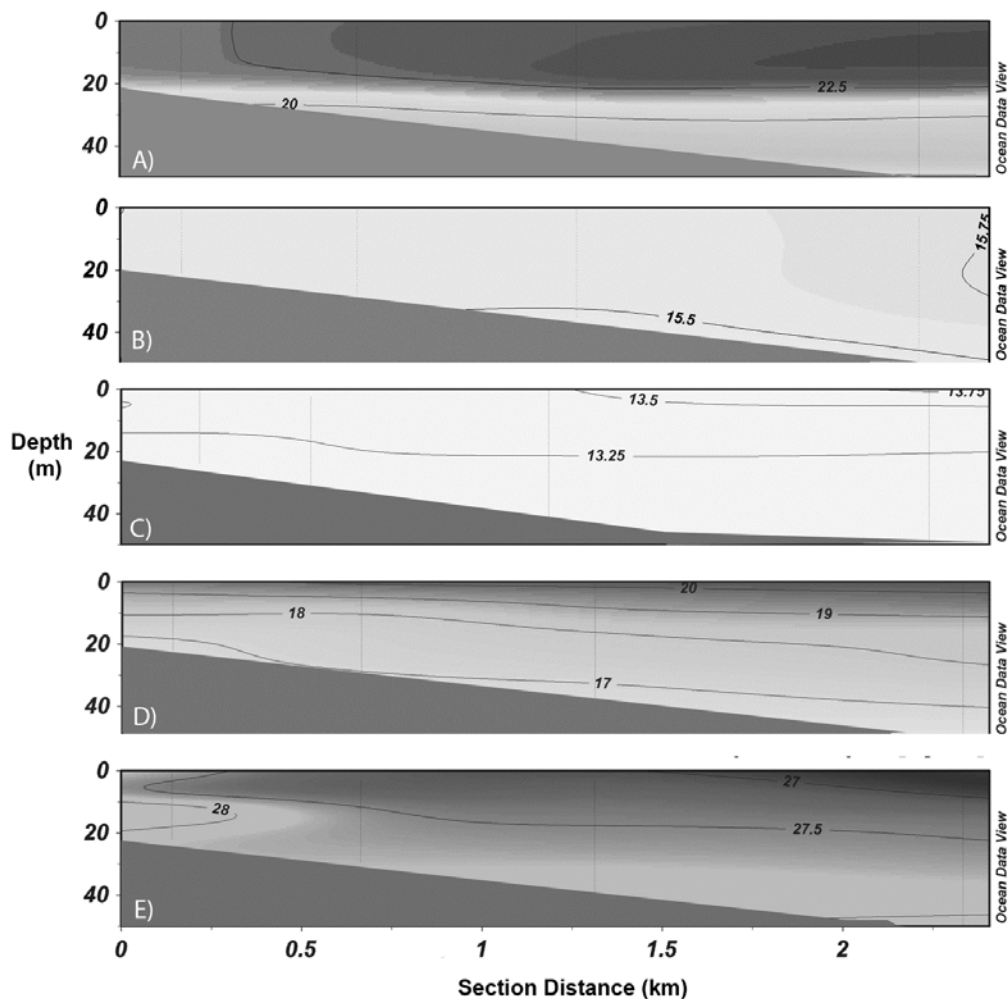
251 Definition of sediment transport events: The sediment transport events during the study
252 period were defined as occurring whenever the magnitude of the instantaneous sediment flux
253 (q) at 20 m water depth exceeded $1.5 \text{ g/m}^2\text{s}$, whereas no-event intervals were defined as
254 times when $q < 0.3 \text{ g/m}^2\text{s}$ (background level). To delimit the beginning and end of the event,
255 a $q > 0.3 \text{ g/m}^2\text{s}$ was used. During an event, peaks of $q < 0.3 \text{ g/m}^2\text{s}$ during less than 24 h
256 were included in the same event. In this manner, sediment transport events were extended
257 to include both resuspension and river sediment supply events along with events of
258 increased current activity.

259 Seabed erosion/deposition: The ALTUS altimeter is an autonomous 2-MHz acoustic
260 transducer coupled with a pressure sensor. This device allows long term monitoring, but is
261 also suitable for high-frequency surveys (sampling frequency up to 1 Hz) and has a data
262 storage capacity of several weeks. The ALTUS provides bed elevation and water level
263 measurements with a resolution of 0.2 and 20 mm, respectively. The transducer was
264 positioned 22 cm above the bed, with a sampling frequency of one measurement every 15
265 minutes. [At all sites, the pressure record for each deployment was also analysed and any](#)
266 [evidence of tripod sinking found was removed from the seabed variation record. Thereby,](#)
267 [any variation of the distance between the sensor and the seabed can be taken as a seabed](#)
268 [deposition/erosion event. However, the pressure sensors at the 30 and 40 m sites were out](#)
269 [of range during the deployments and possible tripod sinking episodes could not be identified.](#)
270 [Thus, at 30 and 40 m depth, seabed deposition was not taken into account and seabed](#)
271 [erosion was treated as minimum erosion.](#)

272 **3. Results**

273 Physical oceanography

274 Masses of water of the studied zone shows the evolution from summer stratified conditions of
275 the water column in September 2007 (Figure 2 A) to the vertical mixing in November 2007
276 and February 2008 (Figure 2 B and C), favoured by the cooling of surface waters and the
277 mixing caused by storm episodes. The final situation of the study period, in spring 2008,
278 corresponds to the onset of the water column stratification (Figure 2 D). The hydrographic
279 structure was also modified by continental freshwater inputs from the Besòs River during the
280 spring season, when the vertical stratification is disturbed in shallow waters (Figure 2 E).



281

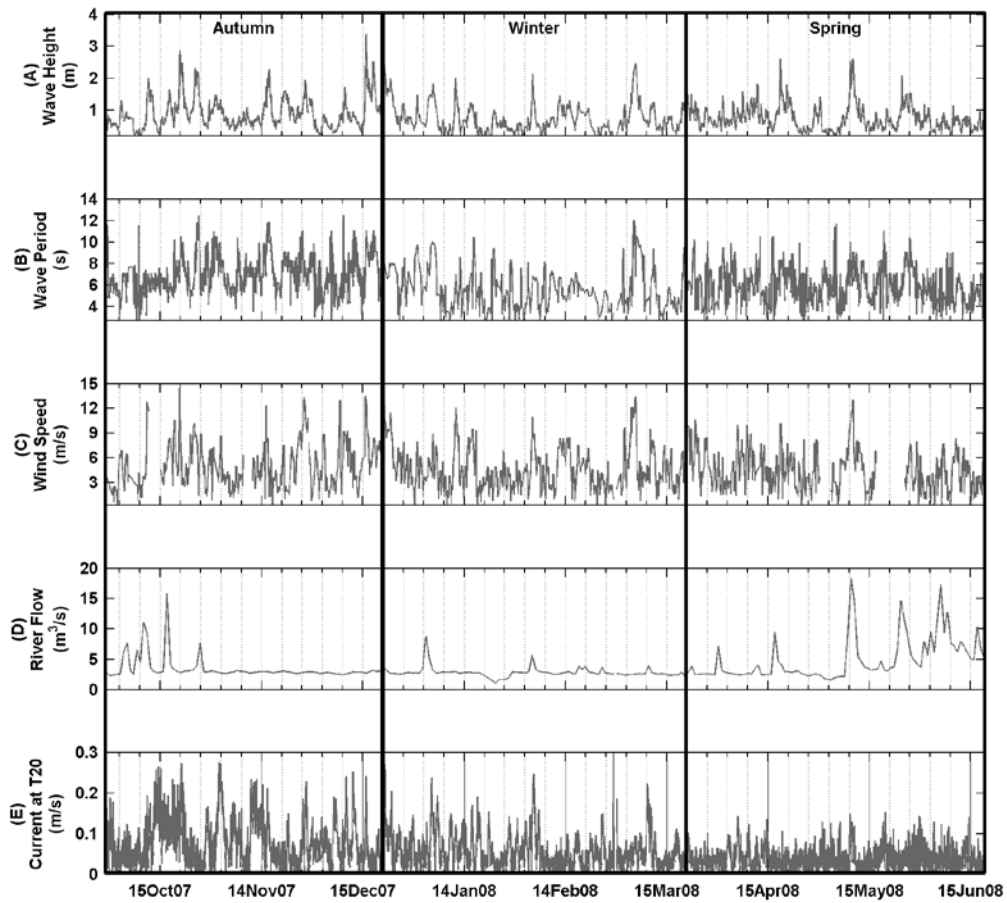
282 *Figure 2. [Across-shelf sections of temperature \(Degrees Celsius\) along the tripods transect in the deployments of](#)*
283 *[\(A\) September 2007. \(B\) November 2007. \(C\) February 2008 and \(D\) June 2008 and \(E\) potential density](#)*
284 *[anomaly \(kg/m³\) at June 2008.](#)*

285 **Waves, winds and river discharge**

286 **Waves:** According to wave measurements, more than 10 storm waves episodes (Hs over 2
287 m and Tp over 9 s) were recorded between autumn 2007 and spring 2008 (Figure 3 A and
288 B). Of the waves propagated, 50% were from the NE-SE, 20% from the SE-S and 28% from
289 the S-SW (Figure 4 A1). [The most energetic episode occurred between 15 and 18 December](#)
290 [2007 and was characterized by a two-peak storm with a maximum peak of Hs of 3.38 m and](#)
291 [a Tp of about 11 s, followed by a smaller storm \(Hs > 2.5 m and Tp > 8 s\) after less than 2](#)
292 [days of relatively calm conditions.](#) Both storm episodes had an eastern component in the
293 direction of wave propagation.

294 **Winds:** Wind reached speeds higher than 12 m/s during most of the storm episodes (Figure 3
295 C), with a blowing direction similar to the direction of wave propagation but slightly rotated
296 (Figure 4), i.e. NE-ESE in the majority of the cases, though a few were from the SW.
297 [Although about another 20% of the wind record fell into the third quadrant \(Figure 4 B2\), no](#)
298 [significant events were associated with these wind directions.](#) In addition, diurnal winds
299 (breezes) were relatively common in early autumn and spring but not correlated with
300 significant wave events, as shown in the across-shelf wind component in Figure 5 A.

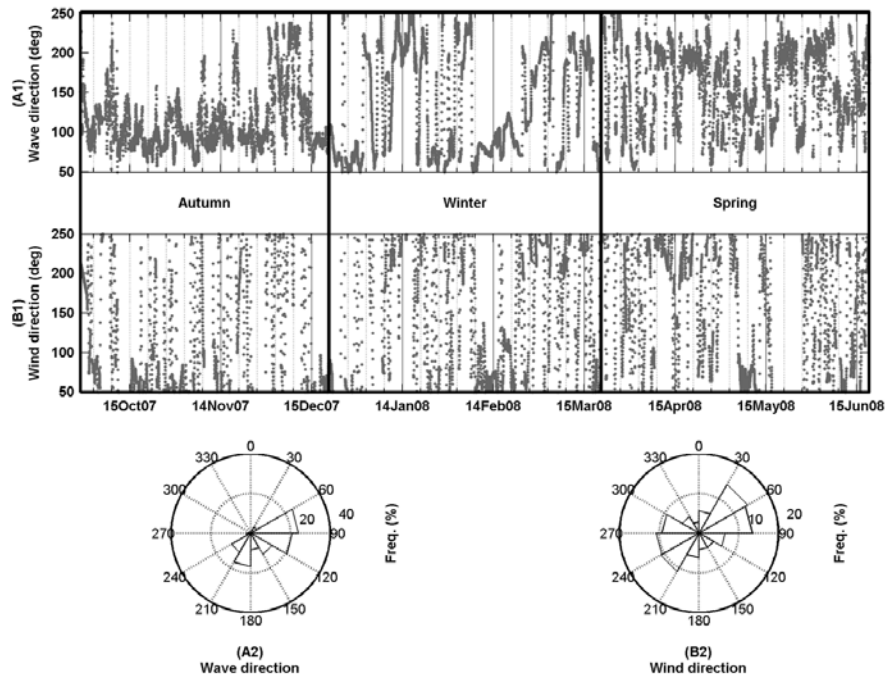
301 **Besòs River discharge:** The Besòs River water discharge measurements showed a typically
302 episodic pattern, with discharge pulses occurring mainly in autumn and spring (Figure 3 D).
303 Average river water discharge during the study period was 3.8 m³/s, with mean daily
304 discharge peaks of 15 and 18 m³/s in October 2007 and May-June 2008, respectively. In
305 October 2007, the increments in river water discharge were characterized by short, fast
306 water pulses accompanied by increases in wave activity. River discharges lasted longer in
307 spring 2008 than in autumn 2007, especially those of June 2008, which occurred under low-
308 energy wave conditions.



309

310
311
312
313

Figure 3. Meteo-oceanographic conditions during the experiment (A) Significant wave height and (B) wave peak period at WANA point 2066051 calibrated with Llobregat buoy data; (C) wind speed at WANA point 2066051; (D) river water discharge at 2.8 km upstream from the Besòs River mouth; and (E) current speed at tripod site T20 (20 m isobath).



314

315 *Figure 4. Time series of wave directions at WANA point 2066051 calibrated with Llobregat buoy data (A1) and*
 316 *wind directions (B1) at WANA point 2066051 during the study period. (A2) and (B2) rose diagram of the relative*
 317 *frequency of the records of wave and wind directions, respectively.*

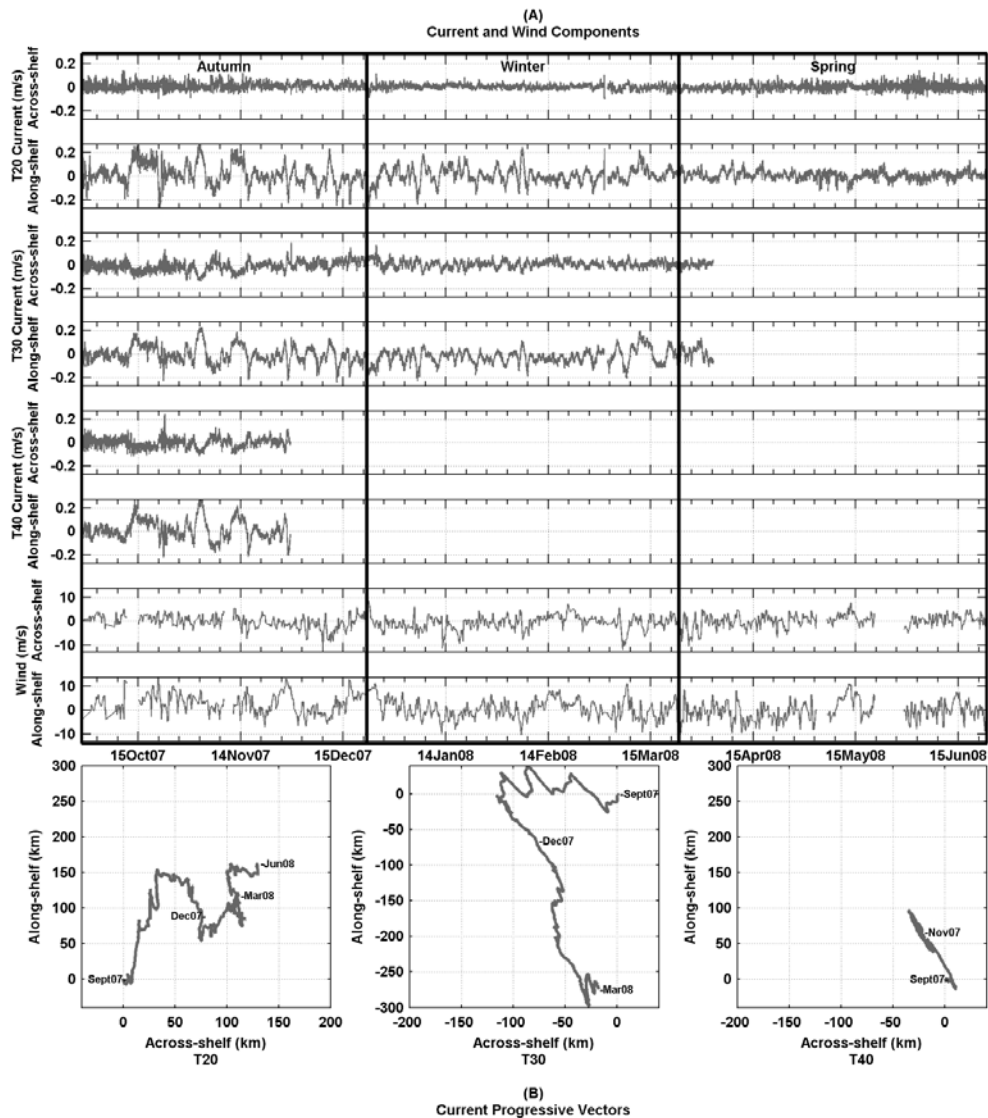
318 **Near-bottom currents**

319 The time series of current speed measured at 0.58 mab from the T20 site (20 m water depth)
 320 is shown in Figure 3 E. At that site, near-bottom current speed averaged 0.071 m/s with
 321 peaks associated with storm wave events on the inner shelf. At the T30 and T40 sites,
 322 current speeds showed similar values (averaged value are 0.056 m/s and 0.067 m/s in T30
 323 and T40 respectively). In the three stations the standard deviation and the maximum current
 324 peaks are similar: 0.045 m/s in T20, 0.044 m/s T30 and 0.056 m/s in T40 for the standard
 325 deviation and peaks up to 0.279 m/s, 0.281 m/s and 0.309 m/s, respectively. In T20, the
 326 current intensity decreases in spring compared to autumn and winter observations (seasonal
 327 averaged intensity is 0.039 m/s).

328 Across the inner shelf, both current components were variable in time during the study
 329 period, particularly the along-shelf component (Figure 5 A). The along-shelf current speed
 330 reached more than 0.20 m/s at all sites in autumn and winter and diminished in intensity in
 331 spring. However, across-shelf velocities were under 0.10 m/s throughout the study period at
 332 T20 and up to 0.15 m/s in autumn and winter at sites T30 and T40 (Figure 5 A). Therefore,

333 evident differences in near-bottom current velocities were found between the T20 site
334 respect to the other sites, where the along-shelf variability was much larger than the across-
335 shelf variability with standard deviations of 0.067 m/s and 0.025 m/s, respectively. While, in
336 the T30 and 40 m T40 sites the across-shelf velocities were stronger and presented more
337 variability, with standard deviations of 0.068 m/s and 0.086 m/s in the along-shelf component
338 and 0.037 and 0.041 in the across-shelf current, respectively. The progressive current
339 vectors shown in Figure 5 B stressed the above-mentioned temporal and spatial variability
340 across the shelf. In autumn (from Sep07 to Dec07 annotations in Figure 5 B), offshore flows
341 controlled the across-shelf component at 20 m water depth, while in deeper waters (sites T30
342 and T40), onshore flows were dominant in the across-shelf direction. At all sites, the resulting
343 along-shelf flows were northeastward in early autumn and southwestward in late autumn.
344 During winter (from Dec07 to Mar08 annotations in Figure 5 B), an evident reversal among
345 the sites in current direction occurred, with the prevalent directed offshore at 20 m depth but
346 southwestward (i.e. along-shelf) at 30 m depth. During this period, the main difference
347 between the two sites was an increase in the along-shelf current intensity at 30 m depth in
348 comparison with the previous period. In spring (from Mar08 to Jun08 in Figure 5 A), at the 20
349 m site the across-shelf current intensity increased progressively, while the along-shelf current
350 intensity decreased during this period. In relation to the direction of the current, both along
351 and across components showed a reversion in the flow direction, northeastward and
352 seaward, respectively.

353 [Although visual correspondence is observed between near-bottom along-shelf flow and the](#)
354 [along-shelf wind direction \(see wind decomposition in Figure 5 A\) during some peaks of the](#)
355 [time series, the current intensity is poorly correlated with the wind with correlation coefficients](#)
356 [under 0.02 for both components at all three sites. The divergence between the wind and the](#)
357 [near-bottom current observations may be originated by several factors such as the role that](#)
358 [play the pressure gradient that may drive the flow under particular circumstances, the](#)
359 [bathymetric effect that modify the flow direction, the role of the stratification that inhibit the](#)
360 [momentum transfer from surface to bottom or the topographic coastal waves \(see discussion](#)
361 [in Grifoll et al., 2012; 2016\).](#)



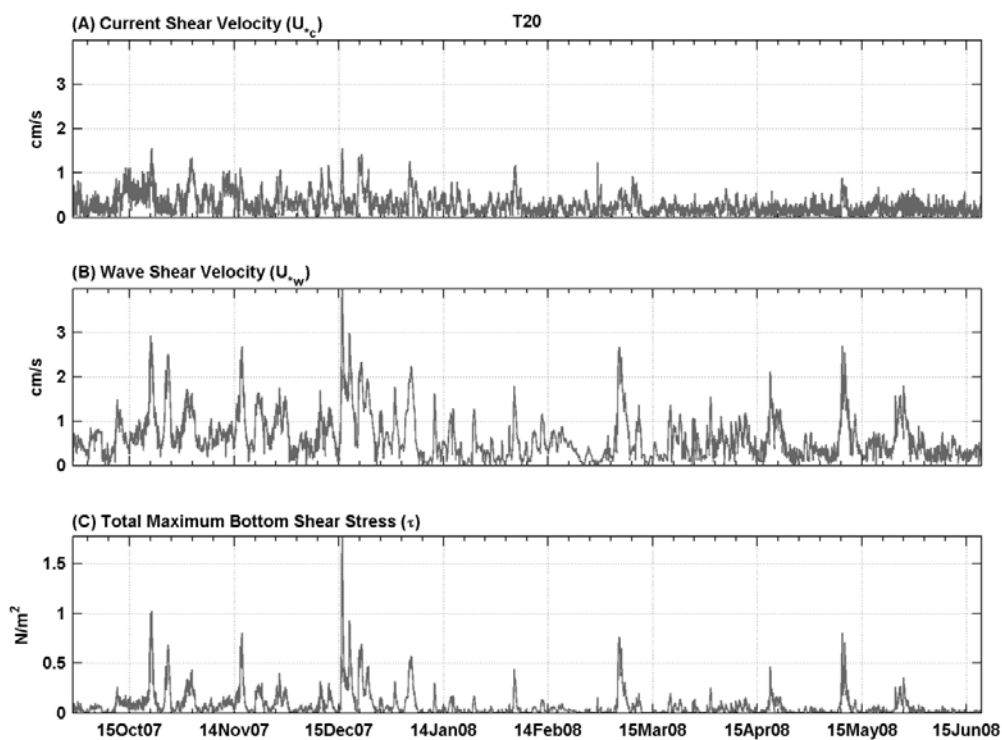
362

363 *Figure 5. (A) Times series of across-shelf and along-shelf near-bottom current and wind components and (B)*
 364 *current progressive vectors in those directions at the T20, T30 and T40 tripod sites, respectively. Positive values*
 365 *are northeastward (along-shelf) and offshore.*

366 **Total maximum bottom shear stress**

367 Estimations of the bottom shear stress reveal that wave-induced stress dominated over
 368 current-induced stress at all sites (Figure 6 at T20 site. T30 and T40 data not shown), with
 369 wave shear velocities (U_w) generally 2 times larger than current shear velocities (U_c) at 20 m
 370 water depth. Comparing periods with available data across the shelf (i.e. October and

371 [November 2007](#)), wave shear stress averaged 0.11 N/m², 0.06 N/m² and 0.04 N/m² and
372 [reached values of 1.02 N/m², 0.43 N/m² and 0.32 N/m² at 20 m, 30 m and 40 m water](#)
373 [depths, respectively. At all sites, autumn 2007 was characterized by a high frequency and](#)
374 [intensity of bottom shear stress. The total maximum bed shear stress was reached during](#)
375 [the 15–18 December 2007 episode, with a maximum peak of 1.77 N/m² at T20 and of 0.99](#)
376 [N/m² at T30. The shear stress decreased significantly in winter and spring 2008, as shown in](#)
377 [the time series at 20 m water depth \(Figure 6\).](#)

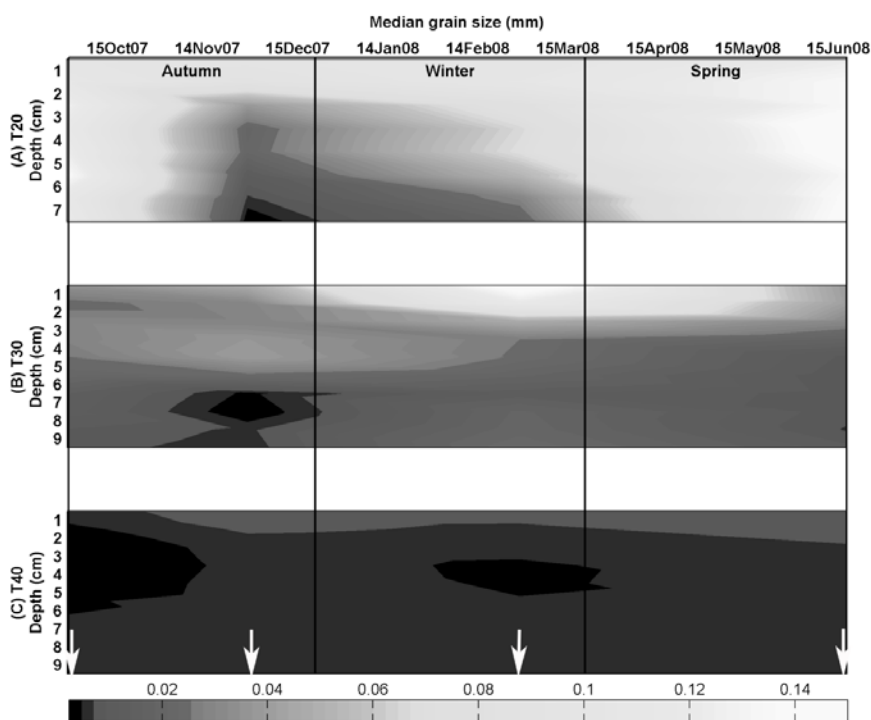


378
379 *Figure 6. Time series at the T20 site (20 m water depth) of: (A) Current Shear Velocities, (B) Wave Shear Velocities*
380 *and (C) Total Bottom Shear Stress.*

381 **Bottom sediment**

382 The bottom sediment grain size displayed a general fining trend from the shallowest site
383 towards the offshore sites, although a high spatial and temporal variability was observed
384 during the study period (Figure 7). At the 20 m water depth site the bottom sediment became
385 finer between September and November 2007 (with median grain sizes changing from 0.12
386 to 0.02 mm) and coarsening during winter, ending in a uniform layer of fine sand (0.14 mm)
387 in spring 2008. At the 30 m site, there was a coarsening trend of the 2-3 surface centimetres

388 from November 2007 to February 2008 ($D_{50}=0.06\text{--}0.14$ mm), ending in a finer quasi-uniform
 389 median grain size distribution in the sediment column in spring 2008 ($D_{50}=0.02\text{--}0.04$ mm).
 390 Finally, no major changes in grain size were observed at the deepest site (40 m depth)
 391 because the grain size variability was within a very fine sediment range ($D_{50}=0.015\text{--}0.025$
 392 mm). However, the observed trend was also a coarsening towards the end of the record
 393 (spring 2008), when the thin layers of clayey sediment detected in previous sampling surveys
 394 (<0.01 mm) disappeared (Figure 7).

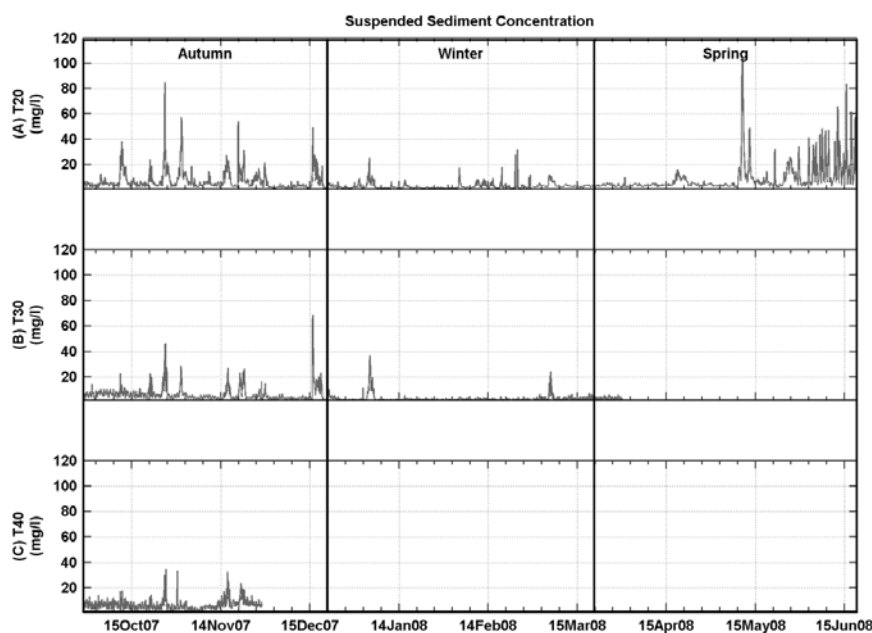


395
 396 *Figure 7. Temporal variability of median grain size (d_{50} in mm) between 0 and 10 cm depth of the cores sampled*
 397 *at 20, 30 and 40 m water depth. White arrows indicate the date when the samples were taken. [The colorbar](#)*
 398 *indicates median grain size in mm.*

399 **Near-bottom suspended sediment concentration**

400 The near-bottom suspended sediment concentration (SSC) during the recording period
 401 showed a high temporal and spatial variability. At the 20 m water depth site, noticeable SSC
 402 was observed in autumn 2007 and spring 2008, with maximum peaks of up to 80 mg/L (25–
 403 26 October 2007) and 100 mg/L (9–10 May 2008), whereas the SSC decreased significantly
 404 in winter, with limited peaks under 40 mg/L. In general, the near-bottom SSC decreased with
 405 depth, with maximum SSC peaks below 70 and 40 mg/L at 30 and 40 m water depth,

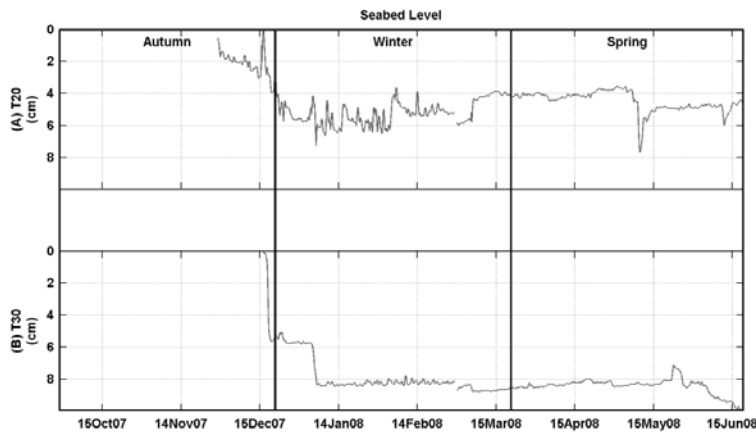
406 respectively. However, SSC was higher at 30 than at 20 m depth during the strongest
407 storms. The 15–18 December 2007 episode generated a SSC of about 70 and 50 mg/L at 30
408 and 20 m water depth, respectively, and the 3–5 January 2008 episode generated an SSC of
409 40 and 20 mg/L at 30 and 20 m water depth, respectively.



410
411 *Figure 8. Time series of SSC at the three tripod sites: (A) T20 at 20 m depth, (B) T30 at 30 m depth, and (C) T40 at*
412 *40 m depth.*

413 **Seabed level**

414 Altimeter data showed a very dynamic seabed, with significant seabed level variability across
415 the inner shelf. Throughout the study period, the shallowest site (20 m depth) showed more
416 dynamism in terms of frequency of erosion/deposition episodes than the 30 m site. However,
417 the net seabed variation during the monitoring period was an erosion of about 4 and 10 cm at
418 20 and 30 m water depth, respectively (Figure 9 A and B). Two major seabed
419 erosion/accumulation episodes related to the strongest storms were recorded at both sites:
420 a) the 15–18 December 2007 episode caused a deposition of a 3 cm layer that was rapidly
421 eroded at the 20 m site and an erosion of more than 6 cm at the 30 m site; and b) the 3–5
422 January 2008 episode caused an erosion of more than 2 and 3 cm at 20 and 30 m depth,
423 respectively.



424

425 *Figure 9. Seabed evolution at (A) the T20 site and (B) the T30 tripod site, at 20 and 30 m water depth,*
 426 *respectively.*

427 **Sediment transport events**

428 Fourteen sediment transport events were identified (Table 2 and Figure 10, see criteria in
 429 Methods): eight in autumn 2008, two in winter 2007-2008 (January–February) and four in
 430 spring 2008 (May–June). Sediment transport events contributed 54% of the total near-bottom
 431 sediment transport and appeared to be roughly proportional to the number of events in each
 432 season. Between September 2007 and June 2008, sediment transport during events ranged
 433 from 70% in autumn, when the majority of the events occurred, to 34% in winter and 53% in
 434 spring. Similar percentages were observed for the along-shelf transport, which represented
 435 70%, 44% and 58% of the total near-bottom transport for these seasons. Indeed, during the
 436 selected events, sediment transport intensity increased in the along-shelf component,
 437 predominantly southwestward, while during no-event intervals the offshore component
 438 prevailed (Figure 11).

439

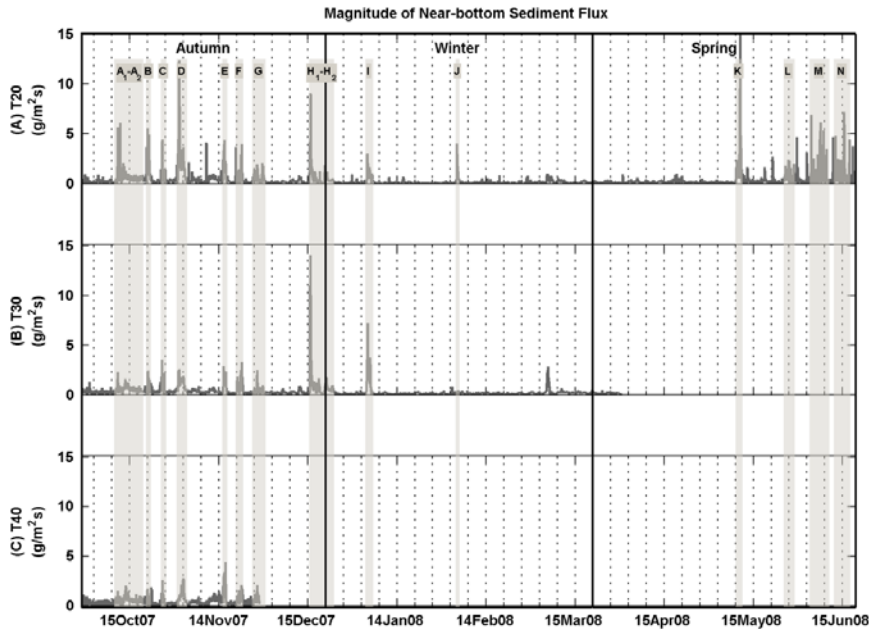
Event	Date: Start / Peak	Duration (h)	Sediment flux (g/m ² s)	U _{br} (m/s)	Wave dir	River water dis. (m ³ /s)	SSC (mg/l)	Current (m/s)		Wind (m/s)		Type of Event
								Speed	Dir	Speed	Dir	
A ₁	11-Oct-07 00:18	29	1.7	<u>0.11</u> 6	96°	4.3	16.7	0.11	128°	10.0	43°	Wet Storm
	11-Oct-07 21:18		6.1	<u>0.33</u> 17	82°	9.1	39.3	0.18	220°	11.1	46°	
A ₂	12-Oct-07 05:38	194	0.6	<u>0.40</u> 06	100°	4.7	5.4	0.13	49°	6.3	56°	Wet Storm
	12-Oct-07 23:58		2.1	<u>0.27</u> 14	101°	15.8	10.2	0.26	43°	10.4	44°	
B	20-Oct-07 18:38	35	1.7	<u>0.25</u> 48	78°	2.8	10.5	0.17	180°	6.3	69°	Ephemeral
	21-Oct-07 07:38		5.6	<u>0.40</u> 72	77°	2.8	22.3	0.24	213°	14.4	59°	
C	25-Oct-07 19:38	36	0.9	<u>0.22</u> 39	88°	4.2	26.3	0.03	143°	5.8	68°	Ephemeral
	26-Oct-07 07:38		4.4	<u>0.60</u> 35	76°	7.7	82.3	0.08	232°	8.8	30°	
D	31-Oct-07 12:58	72	2.4	<u>0.13</u> 24	100°	2.8	16.6	0.16	43°	4.6	49°	Ephemeral
	01-Nov-07 00:58		12.3	<u>0.39</u> 22	132°	2.9	58.0	0.28	56°	8.7	32°	
E	16-Nov-07 01:38	29	2.0	<u>0.26</u> 45	95°	2.9	19.1	0.10	202°	4.5	69°	Ephemeral
	16-Nov-07 12:18		4.4	<u>0.37</u> 62	92°	3.0	27.5	0.21	217°	8.3	9°	
F	20-Nov-07 09:58	56	0.8	<u>0.15</u> 30	98°	3.0	15.9	0.05	175°	3.0	217°	Dry Storm
	22-Nov-07 10:38		3.9	<u>0.21</u> 40	87°	3.0	57.7	0.15	221°	7.5	202°	
G	26-Nov-07 00:18	90	0.7	<u>0.12</u> 24	100°	2.9	8.5	0.08	103°	6.9	77°	Dry Storm
	27-Nov-07 16:58		1.8	<u>0.20</u> 40	83°	3.0	21.6	0.23	216°	13.3	37°	
H ₁	15-dec-07 15:38	93	1.0	<u>0.26</u> 43	89°	3.0	13.0	0.06	167°	7.3	52°	Dry Storm
	15-dec-07 22:58		9.1	<u>0.59</u> 94	87°	3.0	48.9	0.24	224°	13.5	60°	
H ₂	20-dec-07 16:38	74	0.5	<u>0.20</u> 34	84°	3.1	3.5	0.14	222°	10.3	58°	Dry Storm
	21-dec-07 11:58		1.8	<u>0.28</u> 49	109°	3.1	7.8	0.27	217°	13.8	86°	
I	03-jan-08 17:18	61	0.8	<u>0.19</u> 33	104°	3.7	8.0	0.10	187°	5.4	264°	Dry Storm
	04-jan-08 08:18		3.0	<u>0.29</u> 48	55°	6.1	24.1	0.24	219°	8.9	351°	

J	03-Feb-08 22:37	21	1.3	<i>0.13</i> 22	205°	3.8	6.9	0.19	49°	8.9	250°	Dry Storm
	04-Feb-08 03:17		4.0	<i>0.19</i> 32	191°	5.7	17.8	0.25	51°	10.9	202°	
K	09-May-08 12:39	48	2.3	<i>0.21</i> 40	129°	15.0	36.2	0.08	208°	8.8	79°	Wet Storm
	10-May-08 23:38		15.2	<i>0.36</i> 7	131°	18.4	103.7	0.15	201°	13.0	78°	
L	25-May-08 22:19	86	0.6	<i>0.24</i> 12	121°	7.2	15.5	0.04	168°	4.1	227°	Wet Storm
	27-May-08 10:18		2.4	<i>0.23</i> 41	111°	11.8	38.0	0.12	182°	7.7	241°	
M	03-Jun-08 19:39	157	0.6	<i>0.02</i> 3	171°	10.6	17.5	0.03	158°	3.6	159°	River Discharge
	04-Jun-08 07:59		6.9	<i>0.07</i> 44	150°	17.3	47.8	0.13	143°	7.7	240°	
N	12-Jun-08 04:39	129	0.7	<i>0.01</i> 2	159°	6.7	20.5	0.04	113°	3.4	164°	River Discharge
	15-Jun-08 13:59		7.2	<i>0.04</i> 5	212°	10.4	82.1	0.14	53°	7.2	222°	

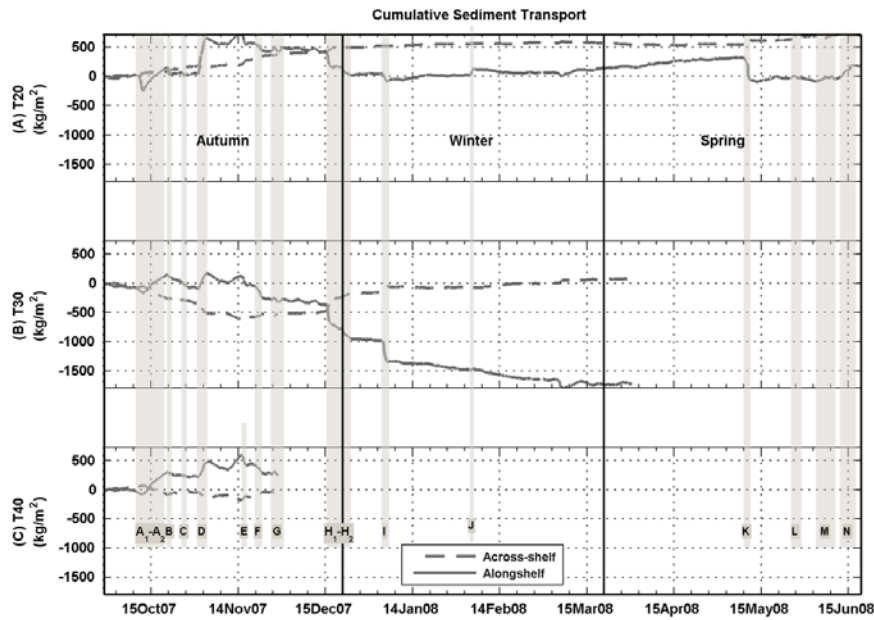
440

441
442
443
444

Table 2. Characteristics of sediment transport events at 20 m water depth from September 2007 to June 2008. Italic and bold numbers correspond to mean and maximum values, respectively. Note that events A and H were divided into two sub-events due to the occurrence of significant changes in the hydrodynamics during these events.



445
446
447 | *Figure 10. Time series of near-bottom sediment flux magnitude at the three tripod locations. (A) 20 m depth, (B)*
448 *30 m depth and (C) 40 m depth. Grey lines and letters indicate the selected sediment flux events defined at the 20*
m depth site.



449
450
451 | *Figure 11. Along-shelf and across-shelf cumulative sediment transport near the bottom for the recording period at*
452 *(A) the 20 m site, (B) the 30 m site and (C) the 40 m site. Positive values northeastward in the along-shelf*
direction and in the offshore direction. Grey lines and letters inside the plots represent the selected events.

453 **4. Discussion**

454 ***SSC and shear stress: Influence of fresh sediment availability***

455 The magnitude of sediment fluxes depends on the across-shelf gradient in wave energy and
456 current speed but also on the availability of suspendable sediment (Harris and Wiberg,
457 2002). On the Barcelona inner shelf, the magnitude of sediment fluxes was clearly influenced
458 by the availability of river-derived fresh sediment and was associated with increases in river
459 discharges, wave and current energy (dry storms), and the coupling of the two processes
460 (wet storms). [This is the reason for the higher SSC at 30 m than a 20 m water depth](#)
461 [observed during some events \(see section 3\)](#). The influence of sediment availability on the
462 magnitude of sediment fluxes can be analysed qualitatively by plotting the relation between
463 the SSC and shear stress during different types of events (Figure 12). An overall relation is
464 derived from the plot, although several conclusions can be drawn when types of sediment
465 flux events are considered. Four types of sediment flux events were differentiated (Table 2):
466 A) high river discharge and low waves (river discharges), B) high river discharge and storm
467 waves (wet storms), C) storm waves with ephemeral bottom layer (ephemeral layers) and D)
468 storm waves (dry storms).

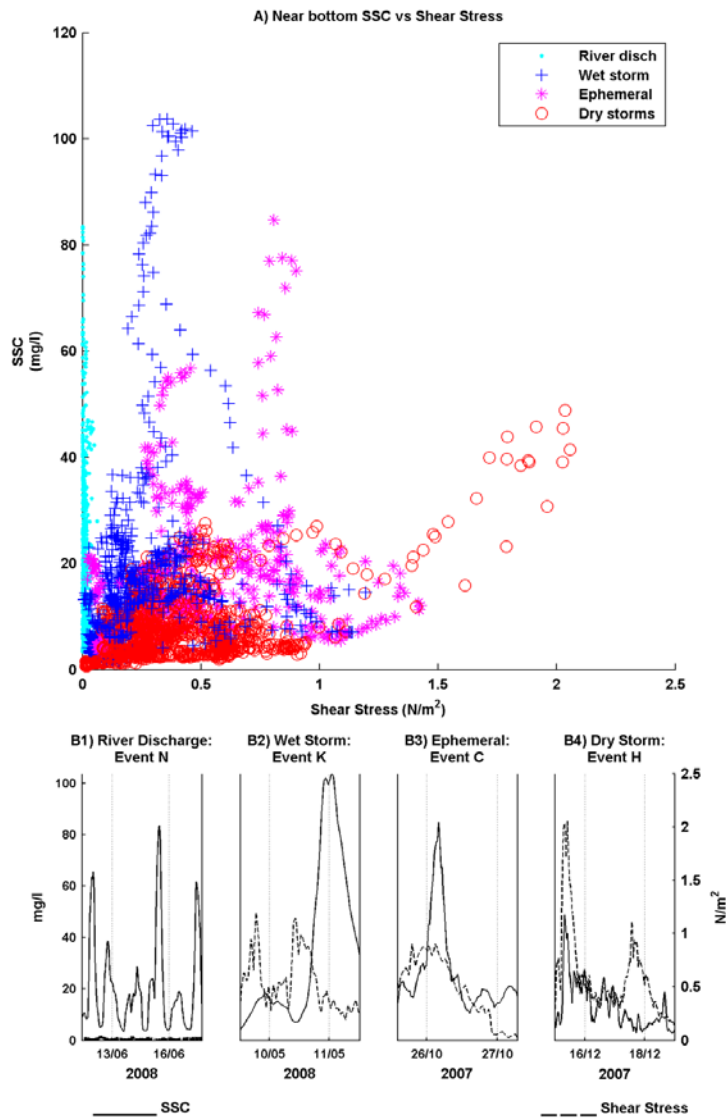
469 The SSC was high during increases in river discharges and very low shear stresses (Figure
470 12 – River Discharges). Under these conditions, a temporal near-bottom nepheloid layer
471 developed where the SSC reached high values (unrelated to shear stress) that lasted as long
472 as the increase in river discharge. Sediment fluxes during these types of event were
473 moderate but long-lasting and accounted for 9% of the total sediment transport during the
474 analysed events.

475 The maximum observed SSC was reached during periods of riverine inputs and moderate
476 wave storms (Figure 12 – Wet Storms). This finding was interpreted as a result of the
477 combination of resuspension processes and the maintenance of a near-bottom nepheloid
478 layer with riverine and bottom particles. In these events, peaks of SSC and shear stress
479 nearly matched. In many cases, an additional peak in the SSC was observed after the
480 maximum peak of the storm (Figure 12 B) due to the advection of riverine sediment, as
481 observed on other shelves (Ogston and Sternberg, 1999). Sediment fluxes during wet storms
482 accounted for 38% of the total sediment transport during events. Indeed, the most
483 noteworthy sediment transport event occurred under a wet storm that was not the most
484 energetic event in terms of shear stress.

485 The availability of fresh sediment through the formation of ephemeral bottom layers also
486 affected the magnitude of SSC and sediment fluxes during some intermediate-intensity
487 storms during the study period. The formation of flood-derived fine deposits offshore of the
488 Besòs River system previous to a storm passage could enhance the bottom sediment
489 erodibility and SSC because of the higher porosity and water content of the fresh sediment
490 (Grifoll et al., 2014; Guillén et al., 2006). During these events, the presence of ephemeral
491 layers changed bottom sediment erodibility and SSC reached higher values than expected
492 due to wave-current conditions (Figure 12 – Ephemeral). The influence of these ephemeral
493 layers, and therefore of river-derived fresh sediment, was observed in both shallow and
494 deeper inner shelf waters. Once the fresh sediment was eroded and transported offshore,
495 the available fresh sediment, now in deeper areas, increased the SSC in comparison with
496 shallow waters, changing the across-shelf gradient of sediment fluxes (higher sediment flux
497 in deeper water during events H and I – Figure 10). Sediment fluxes during events influenced
498 by ephemeral layers accounted for 29% of the total transport during events.

499 Finally, the maximum shear stress occurred during dry storms events, in which SSC and
500 shear stress peaks coincided (Figure 12 D), suggesting that resuspension of bottom
501 sediment controls SSC. The near-bottom sediment flux during dry storms accounted for 24%
502 of the total sediment transport during events.

503 Actually, the proportionality between SSC and shear stress is observed when individual wave
504 storms events are considered. However, this proportionality disappears when all events are
505 taken into account, mainly because of changes in conditions of fresh sediment availability.
506 The influence of fresh sediment availability in sediment dynamics can be evaluated in terms
507 of the percentage of suspended sediment fluxes with or without available fresh sediment
508 (river discharges or ephemeral layers), which accounted for 76% of the sediment transport
509 events. In fact, only 5 of the 14 defined sediment transport events occurred without a direct
510 influence of riverine inputs.



511

512 *Figure 12. A) The relation between suspended sediment concentration (SSC) and bottom shear stress according to*
 513 *the four types of sediment transport events identified on the Barcelona inner shelf: high river discharge and low*
 514 *waves, wet storms, storms with ephemeral bottom layers, and dry storms. B1, B2, B3 and B4) Time series of SSC,*
 515 *shear stress and river discharge for one of each type of sediment transport events.*

516 **Seasonality of sediment dynamics**

517 The resulting near-bottom sediment transport on the Barcelona inner shelf off the Besòs
 518 River was mainly directed southwestward (along-shelf) during the study period. This fact is
 519 consistent with previous observations on low-energy shelves, where along-shelf sediment
 520 flux is stronger than across-shelf flux, in contrast to high-energy shelves (Allison et al., 2000;

521 Fain et al., 2007; Ogston and Sternberg, 1999; Ogston et al., 2000; Palanques et al., 2002;
 522 Sherwood et al., 1994; Traykovski, et al., 2000;). The seaward component of sediment flux
 523 on the Besòs shelf was indeed low but favoured the segregation of coarse and fine sediment
 524 from the nearshore towards deeper waters, as observed in the temporal variability of the
 525 sediment grain size across the inner shelf (Figure 7). In fact, previous studies carried out in
 526 the area described a mud belt between 30 and 60 m water depth that was shifted
 527 southwestward by the dominant along-shelf transport (Checa et al., 1988; Liqueste et al.,
 528 2007; Grifoll et al., 2014; Palanques and Díaz, 1994).

529 However, the sediment dynamics of “small” Mediterranean river systems such as the one
 530 studied show a seasonal variability (Guillén et al., 2006). In the Besòs River system, the
 531 temporal variation of the hydrographic structure, the magnitude of the forcing conditions, the
 532 observed SSC and fluxes, and the seabed evolution indicate strong seasonal variability in
 533 sediment dynamics controlled by the type, frequency and intensity of sediment transport
 534 events. Wet storms events occurred basically in autumn and spring while in winter, dry
 535 storms were the main forcing mechanism for sediment transport. Consequently, the
 536 averaged near-bottom sediment fluxes were higher in autumn and spring than in winter
 537 during the study period (Table 3). The seasonal variability is also evident in the distribution of
 538 the across-shelf magnitude of sediment fluxes, which decrease and increase between 20
 539 and 30 m water depth in autumn and winter, respectively.

NEAR- BOTTOM FLUXES	TYPE OF EVENTS							SEASONS				
	Wet storm	Ephemeral			Dry storm		River Disch.	Autumn		Winter		Spring
	20 m	20 m	30 m	40 m	20 m	30 m	20 m	20 m	30 m	20 m	30 m	20 m
Mean along- shelf flux	1.63	1.79	0.94	0.84	0.69	0.91	0.40	0.47	0.38	0.14	0.19	0.22
Mean across- shelf flux	0.88	0.39	0.49	0.34	0.15	0.43	0.37	0.14	0.22	0.04	0.08	0.16
Averaged flux	2.07	1.90	1.09	0.92	0.74	1.03	0.60	0.52	0.46	0.15	0.22	0.29
Net flux	320	268	109	45	379	795	200	425	694	61	822	114
Net direction	125	112	47	135	149	159	136	60	208	47	153	66

540

541 *Table 3. Near-bottom sediment fluxes: Mean and averaged sediment flux-in ($\text{g}/\text{m}^2\text{s}$) and net flux magnitude (g/m^2*
542 *for the specific time interval) and direction (degrees) with respect to north at the tripod locations, for each type*
543 *of event and by season.*

544 This temporal and spatial distribution of sediment fluxes on the Barcelona inner shelf is
545 analysed as follows through the description of sediment dynamics in autumn, winter, spring
546 and summer.

547 Autumn

548 The pattern of sediment dynamics in autumn 2007 was characterized by early riverine inputs
549 that formed ephemeral sediment layers on the inner shelf, with subsequent resuspension
550 and partial offshore transport at 20 m water depth, which mainly switched southwestward
551 between 30 and 40 m water depth until resuspendable sediment was depleted. The along-
552 shelf transport was twice as high as the across-shelf transport but the predominant offshore
553 component in late autumn favoured the dispersion of riverine sediments towards deeper
554 water. At the beginning of this season, the strong stratification in the water column and the
555 combined action of moderate waves and currents resulted in a convergence of the sediment
556 flux between 20 and 30 m water depth. Thus, the spread of the riverine sediment was
557 prevented, probably leaving a deposit of fresh sediment in shallow waters that allowed the
558 instantaneous sediment flux to reach values of about $12 \text{ g}/\text{m}^2\text{s}$ at the shallowest site (20 m
559 depth), while at 30 and 40 m water depths it was under $5 \text{ g}/\text{m}^2\text{s}$ (event D – Figure 10). In the
560 subsequent storm events sediment fluxes were lower than expected considering bottom
561 shear stress probably because the ephemeral sedimentary layer was already eroded..

562 Winter

563 Winter conditions in 2008 were characterized by a homogeneous water column, low river
564 water discharges and moderate wave activity. Two wave storm episodes with prevailing
565 northeasterly winds that favoured stronger along-shelf over across-shelf flow (events I and J)
566 lasted 2 days and 1 day, respectively. The pattern of sediment transport was similar to that in
567 late autumn 2007, with limited fine-grained sediment in shallow waters and sediment
568 transport predominantly towards the southwest. The variability in the intensity of sediment
569 fluxes across the shelf is consistent with the seabed changes observed during this season,
570 (Figure 7 and 9). The across-shelf bottom sediment distribution caused the excess of shear
571 stress to increase offshore during this event and, consequently, sediment fluxes were higher
572 at 30 than at 20 m water depth ($7 \text{ g}/\text{m}^2\text{s}$ and $3 \text{ g}/\text{m}^2\text{s}$, respectively), with a prevalent near-
573 bottom southwestward current at both sites.

574 **Spring**
575 Spring 2008 was characterized by the onset of the stratified conditions of the water column,
576 moderate winds and waves, and prolonged high river water discharge. The river discharge
577 and wind regime were typical of those occurring during the Mediterranean spring season
578 (Cerralbo et al., 2015; Font, 1990; Liqueste et al., 2009;), with a predominant southeasterly
579 wind direction during low-pressure system passages and sea breezes in the diurnal bands.
580 However, the spring 2008 events were characterized by moderate wind energy in both
581 frequency bands. Seabed variations and sediment flux measurements from May to June
582 2008 suggest a multi-step deposition-erosion-transport pattern across the inner shelf. The
583 mechanisms responsible for the high sediment transport at 20 m water depth (in relation to
584 moderate shear stress) may be related to the high river flow (up to 5 m³/s) between May and
585 June 2008, which could have contributed to the maintenance of high SSC in the water
586 column and the formation of an ephemeral sediment layer progressively migrating offshore.
587 In June 2008, the thermocline was around 30 m depth and was associated with high near-
588 bottom SSC (Figure 2 D). It could therefore be hypothesized, as suggested in previous
589 studies (Puig et al., 2001; 2007; Urgelés et al., 2011), that processes linked to the
590 thermocline such as internal waves favour bottom sediment remobilization and the
591 maintenance of a bottom nepheloid layer.

592 **Summer**

593 Although no full observations were obtained in summer 2008, the Mediterranean climate is
594 characterized by dry summers with well-developed sea breezes (Cerralbo et al., 2015; Font,
595 1990) and relatively stable atmospheric conditions. In summer 2008, measured wave
596 conditions below a significant wave height of 1.3 m and mean river water discharge (2.31
597 m³/s) were consistent with the summer season in the area (Bolaños et al., 2008; Sánchez-
598 Arcilla et al., 2008). Thermal stratification developed on the shelf due to the increase in heat
599 fluxes, as occurred seasonally (Grifoll et al, 2014; Salat et al. 2002). In consequence, under
600 these conditions we can infer that significant sediment transport events were not expected
601 during the summer period.

602 **5. Conclusions**

603 This study shows the complexity of “small” Mediterranean river systems in the sediment
604 dispersal from the continent to the sea. This complexity gives rise to a set of sediment
605 resuspension and transport mechanisms with a strong seasonal variability. In early autumn,
606 evidence of the formation of temporal nepheloid layers and ephemeral sediment bottom

607 layers was found, indicating increased availability of fine sediment near the bottom to interact
608 with resuspension and transport processes. In late autumn and winter events, high bed shear
609 stresses and prevalent southwestern and offshore currents resuspended and winnowed the
610 ephemeral layers previously deposited in shallow waters. In spring, large river discharge
611 episodes were more frequent, and most of them occurred under low-energy wave conditions.
612 In these cases additional processes such as diurnal winds and/or hydrographic conditions
613 may have controlled sediment transport. This seasonal variability leads to a temporal
614 evolution of the bottom grain size (coarser during winter) and the near-bottom sediment
615 transport rates (higher in autumn and spring), which are consistent with the hydrodynamic
616 seasonal events and the river discharge regime.

617 [In the Besòs River system, more than 50% of the total near-bottom suspended sediment](#)
618 [transport from September 2007 to July 2008 occurred in 14 storm events, which represented](#)
619 [the 54 % of the total sediment transport along the study period. The contribution of the](#)
620 [events, however, differed along each season, which represented the 70 %, 34 % and 53 % in](#)
621 [autumn, winter and spring, respectively.](#) Of these events, about 75% were directly influenced
622 by riverine inputs through temporal nepheloid layers and/or ephemeral bottom layers,
623 highlighting the importance of the availability of fresh riverine sediment in near-bottom
624 suspended sediment transport rates across the inner shelf. In general, sediment transport
625 and seabed changes were lower when riverine fresh sediment was not available across the
626 inner shelf. Nonetheless, when riverine sediment was available in the nearshore, sediment
627 transport rates were enhanced in shallow waters (20 m water depth) and the across-shelf
628 sediment transport rate decreased offshore. In contrast, when fresh sediment had been
629 winnowed from shallow areas (20 m water depth) and deposited offshore (30 m water depth),
630 sediment transport and seabed erosion were higher offshore as the sediment availability
631 increased there.

632 These results show that small rivers delivering sediment into the Mediterranean basin
633 enhance near-bottom suspended sediment transport rates by increasing the SSC and
634 decreasing threshold conditions for bottom sediment resuspension. [In the Mediterranean](#)
635 [almost tideless area with weak currents, river discharge and wave climate control the](#)
636 [availability of sediment to be resuspended and transported to other parts of the inner-shelf.](#)
637 [Both of these controlling factors are seasonal, so sediment dynamics on the inner shelf also](#)
638 [displays seasonality.](#)

639 **Acknowledgements**

640 This work was supported by the *Ministerio de Educación y Ciencia* of the Spanish
641 Government within the SEDMET project (CTM2006-06919). The authors would like to thank
642 Óscar Ferreira (CIMA-UALG, Portugal) and Henko de Stigter (NIOZ, the Netherlands) for
643 their comments and suggestions on an initial draft. The manuscript was also improved by
644 suggestions from all members of the committee for the defence of the doctoral thesis in
645 which this paper was presented among other results. The research leading to these results
646 obtained data from the *Xarxa d'Instrumentes Oceanogràfics i Meteorològics (Generalitat de*
647 *Catalunya)*, which is currently out of service. We also thank the officers and crew of the R/V
648 *García del Cid* (CSIC) and the R/V *Sarmiento de Gamboa* (MINECO) and the staff of the
649 *Institut de Ciències del Mar* (CSIC) and the *Unitat de Tecnologia Marina* (CSIC) for their help
650 and dedication during the cruises and in the laboratory work. L.L, A.P. and J.G belong to
651 CRG on Littoral and Oceanic Processes, supported by Grant 2014 SGR 1642 of the
652 *Generalitat de Catalunya*.

653 **References**

654 Allison, M.A., Kineke, G.C., Gordon, E.S. and Goñi, M.A. (2000). Development and reworking of a seasonal flood deposit on the
655 inner continental shelf off the Atchafalaya River. *Continental Shelf Research* 20, 2267–2294.

656 Antonijuan, J., Guillén, J., López, L. and Simarro, G. (2012). Near-bottom sediment dynamics on highly-protected beaches The
657 Coastal Ocean Observatory of Barcelona. *IEEE Instrumentation and Measurement Technology Conference 2012*, 403
658 – 406.

659 Bever, A.J., McNinch, J.E. and Harris, C.K. (2011). Hydrodynamics and sediment-transport in the nearshore of Poverty Bay,
660 New Zealand: Observations of nearshore sediment segregation and oceanic storms. *Continental Shelf Research* 31,
661 507–526.

662 Bolaños, R., Jorda, G., Cateura, J., Lopez, J., Puigdefabregas, J., Gomez, J. and Espino, M. (2008) The XIOM: 20 years of a
663 regional coastal observatory in the Spanish Catalan coast. *Journal of Marine Systems* 77, 237–260.

664 Bolaños, R., Wolf, J., Brown, J., Osuna, P., Monbaliu, J., and Sanchez-Arcilla, A., (2009). Comparison of wave-current
665 interaction formulation using the POLCOMS-WAM wavecurrent model, *Coastal Engineering*, World Scientific
666 Publishing, 521–533.

667 Bourrin, F., Friend, P.L., Amos, C.L., Manca, E., Ulses, C., Palanques, A., Durrieu de Madron, X. and Thompson, C.E.L. (2008).
668 Sediment dispersal from a typical Mediterranean flood: The Têt River, Gulf of Lions. *Continental Shelf Research* 28,
669 1895–1910.

670 Cacchione, D.A., Drake, D.E., Kayen, R.W., Sternberg, R.W., Kineke, G.C. and Tate, G.B. (1995). Measurements in the bottom
671 boundary layer on the Amazon subaqueous delta. *Marine Geology* 125, 235–257.

672 Catalan Water Agency. Agència Catalana de l'Aigua (Generalitat de Catalunya). Consulta de dades de l'aigua i el medi
673 (CDAM). Estació d'aforament de Santa Coloma de Gramenet (riu) (EA047). <http://aca-web.gencat.cat/sdim/visor.do>,
674 Last accessed: March 2016.

675 Cerralbo, P., Grifoll, M., Moré, J., Bravo, M., Sairouni Afif, A. and Espino, M. (2015). Wind variability in a coastal area (Alfacs
676 Bay, Ebro River delta). *Advances in Science and Research* 12, 11–21.

677 Checa, A., Díaz, J.I., Farrán, M., Maldonado, A., (1988). Sistemas deltaicos holocenos de los ríos Llobregat, Besòs y Foix:
678 modelos evolutivos transgresivos. *Acta Geològica Hispànica*. 23, 241–255.

679 Dufois, F., Verney, R., LeHir, P., Dumas, F. and Charmasson, S. (2014) Impact of winter storms on sediment erosion in the
680 Rhone River prodelta and fate of sediment in the Gulf of Lions (North Western Mediterranean Sea). *Continental Shelf*
681 *Research* 72 , 57–72.

682 Fain, A.M.V, Ogston, A.S. and Sternberg, R.W. (2007). Sediment transport event analysis on the western Adriatic continental
683 shelf. *Continental Shelf Research* 27, 431 – 451.

684 Ferré, B., Guizien, K., Durrieu de Madron, X., Palanques, A., Guillén, J., Grémare, A. (2005). Fine-grained sediment dynamics
685 during a strong storm event in the inner-shelf of the Gulf of Lion (NW Mediterranean). *Continental Shelf Research* 25,
686 2410–2427.

687 Flexas, M.M., Durrieu de Madron, X., García, M.A., Canals, M. and Arnau, P. (2002). Flow variability in the Gulf of Lions during
688 the MATER HFF experiment (March–May 1997). *Journal of Marine Systems* 33–34, 197–214.

689 Font, J. (1990). A comparison of seasonal winds with currents on the continental slope of the Catalan Sea (northwestern
690 Mediterranean). *Journal of Geophysical Research* 95 (C2), 1537–1545.

691 Geyer, W.R., Hill, P., Milligan, T., Traykovski, P. (2000). The structure of the Eel River plume during floods. *Continental Shelf*
692 *Research* 20, 2067–2093.

693 Giró, S. and Maldonado, A. (1985). Análisis granulométrico por métodos automáticos: tubo de sedimentación y Sedigraph. *Acta*
694 *Geològica Hispànica* 20, 95-102.

695 Grifoll, M., Aretxabaleta, A. L., Espino, M. and Warner, J. C. (2012). Along-shelf current variability on the Catalan inner-shelf
696 (NW Mediterranean). *Journal Geophysical Research: Oceans (1978–2012)* 117 (C9).

697 Grifoll, M., Gracia, V., Fernandez, J. and Espino, M. (2013_1). Suspended sediment observations in the Barcelona inner-shelf
698 during storms. *Journal Coastal Research, Special Issue* 65, 1533-1538.

699 Grifoll, M., Aretxabaleta, A. L., Pelegrí, J.L., Espino, M., Warner, J. C. and Sánchez-Arcilla, A. (2013_2). Seasonal circulation
700 over the Catalan inner-shelf (northwest Mediterranean Sea). *Journal Geophysical Research: Oceans* 118, 10, 5844-
701 5857.

Formatat: espanyol (Espanya - alfab. tradicional)

Formatat: espanyol (Espanya - alfab. tradicional)

Formatat: anglès (EUA)

Formatat: anglès (EUA)

Formatat: anglès (EUA)

- 702 Grifoll, M., Gracia, V., Aretxabaleta, A., Guillén, J., Espino, M. and Warner, J.C. (2014). Formation of fine sediment deposit from
703 a flash flood river in the Mediterranean Sea. *Journal Geophysical Research: Oceans* 119, 5837-5853.
- 704 Gómez J., Espino, M., Puigdefabregas, J., Jerez, F. (2005). Xarxa d'Instrumentació Oceanogràfica i Meteorològica de la
705 Generalitat de Catalunya (XIOM). Boies d'onatge dades obtingudes l'any 2004. Informe Tècnic.
- 706 Guillén, J., Palanques, A., Durrieu de Madron, X., Nyffeler, F. (2000). Field calibration of optical sensors for measuring
707 suspended sediment concentration in the western Mediterranean. *Scientia Marina* 64 (4), 427-435.
- 708 Guillén, J., Jiménez, J.A., Palanques, A., Gràcia, V., Puig, P., Sánchez-Arcilla, A. (2002). Sediment resuspension across a
709 microtidal, low-energy inner-shelf. *Continental Shelf Research* 22, 305-325.
- 710 Guillén, J., Bourrin, F., Palanques A., Durrieu de Madron X., Puig P. and Buscail R. (2006). Sediment dynamics during wet and
711 dry storm events on the Têt inner-shelf (SW Gulf of Lions). *Marine Geology* 234 (1-4), 129-142.
- 712 Harris, C.K. and Wiberg, P.L. (1997). Approaches to quantifying long-term continental shelf sediment transport with an example
713 from the Northern California STRESS mid-shelf site. *Continental Shelf Research* 17 (11), 1387-1418.
- 714 Harris, C.K. and Wiberg, P.L. (2002). Across-shelf sediment transport: Interactions between suspended sediment and bed
715 sediment. *Journal of Geophysical Research* 107 (C1).
- 716 ITGE (1989). Mapa geològic de la plataforma continental espanyola y zonas adyacentes, 1 :200000. Hoja 35/ 42A, Barcelona.
717 Instituto Tecnològic GeoMinero de España, Madrid, mem. Expl, pp. 117.
- 718 Jiménez, J.A., Guillén, J., Gracia, V., Palanques, A., García, M.A., Sánchez-Arcilla, A., Puig, P., Puigdefabregas, J. and
719 Rodríguez, G. (1999). Water and sediment fluxes on the Ebro Delta shoreface: on the role of low frequency currents.
720 *Marine Geology* 157, 219-239.
- 721 Liqueste, C., Canals, M., Lastres, G., Amblas, D., Urgelès, R., De Mol, B., De Batis, M., Hughes-Clarke, J.E. (2007). Long-term
722 development and current status of the Barcelona continental shelf: a source-to-sink approach. *Continental Shelf*
723 *Research* 27, 1779-1800.
- 724 Liqueste, C., Canals, M., Ludwig, W., Arnau, P., (2009). Sediment discharge of the rivers of Catalonia, NE Spain, and the
725 influence of human impacts. *Journal of Hydrology* 366, 76-88.
- 726 Liqueste, C., Lucchi, R.G., Garcia-Orellana, J., Canals, M., Masque, P., Pascual, C. and Lavoie, C. (2010). Modern
727 sedimentation patterns and human impacts on the Barcelona continental shelf (NE Spain). *Geologica Acta* 8 (2), 169-
728 187.
- 729 Liste, M., Grifoll, M., and Monbaliu, J. (2014). River plume dispersion in response to flash flood events. Application to the
730 Catalan shelf. *Continental Shelf Research* 87, 96-108.
- 731 Ogston, A.S. and Sternberg, R.W., (1999). Sediment transport events on the northern California continental shelf. *Marine*
732 *Geology* 154, 69-82.
- 733 Ogston, A.S., Cacchione, D.A., Sterberg, R.W., Kineke, G.C. (2000). Observations of storm and river flood-driven sediment
734 transport of the northern Californian continental shelf. *Continental Shelf Research* 20, 2141-2162.
- 735 Palanques, A., Plana, F., and Maldonado, A. (1990). Recent influence of man on Ebro margin sedimentation system
736 (Northwestern Mediterranean sea). *Marine Geology* 95, 247-63.
- 737 Palanques, A. (1994). Distribution and heavy metal pollution of the suspended particulate matter on the continental shelf (North-
738 Western Mediterranean). *Environmental Pollution* 85, 205-215.
- 739 Palanques, A. and Diaz, J.I. (1994). Anthropogenic heavy metal pollution in the sediment of the Barcelona continental shelf
740 (Northwestern Mediterranean). *Marine Environmental research* 38, 17-31.
- 741 Palanques, A., Puig, P., Guillén, J., Jiménez, J., Gràcia, V., Sánchez Arcilla, A., Madsen, O. (2002). Near-bottom suspended
742 sediment fluxes on a river-influenced, tideless fetch-limited shelf (the Ebro continental shelf, NW Mediterranean).
743 *Continental Shelf research* 22 (2), 285-303.
- 744 Palanques, A., Guillén, J., Puig, P., and Durrieu de Madron, X. (2008). Storm-driven shelf-to-canyon suspended sediment
745 transport at the southwestern end of the Gulf of Lions, *Continental Shelf Research* 28, 1947-1956.
- 746 Palanques, A., Puig, P., Guillén, J., Durrieu de Madron, X., Latasa, M., Scharek, R. and Martin, J. (2011). Effects of storm
747 events on the shelf-to-basin sediment transport in the southwestern end of the Gulf of Lions (Northwestern
748 Mediterranean). *Nat. Hazards Earth Syst. Sci.* 11, 843-850.
- 749 Pallares, E., Sánchez-Arcilla, A. and Espino, M. (2014) Wave energy balance in wave models (SWAN) for semi-enclosed
750 domains – Application to the Catalan coast. *Continental Shelf Research* 87, 41-53.

Formatat: anglès (EUA)

Formatat: anglès (EUA)

- 751 Puig, P. and Palanques, A. (1998). Nepheloid structure and hydrographic control in the Barcelona continental margin. *Marine*
752 *Geology* 149, 39–54.
- 753 Puig, P., Palanques, A., Sánchez-Cabeza, J.A., Masqué, P. (1999). Heavy metals in particulate matter and sediments in the
754 southern Barcelona sedimentation system (Northwestern Mediterranean). *Marine Chemistry* 63, 311-329.
- 755 Puig, P., Palanques, A., Guillén, J. (2001). Near-bottom suspended sediment variability caused by storms and near-inertial
756 internal waves on the Ebro mid continental shelf (NW Mediterranean). *Marine Geology* 178, 81-93.
- 757 Puig, P., Ogston, A.S., Guillen, J., Fain, A.M.V. and Palanques, A. (2007). Sediment transport processes from the topset to the
758 foreset of a crenulated clinoform (Adriatic Sea). *Continental Shelf Research* 27, 452–474.
- 759 Roussiez, V., Aloisi, J.C., Monaco, A. Ludwig, W. (2005). Early Buddy deposits along the Gulf of Lions shoreline: a key for
760 better understanding of land-to-sea transfer of sediments and associated pollutant fluxes. *Marine Geology* 222-223,
761 345-358.
- 762 Rubio, A., Arnau, P.A., Espino, M., Flexas, M., Jordà, G., Salat, J., Puigdefàbregas, J. and Arcilla, A.S. (2005). A field study of
763 the behaviour of an anticyclonic eddy on the Catalan continental shelf (NW Mediterranean), *Progress in*
764 *Oceanography* 66, 142–156.
- 765 Salat, J., García, M. A., Cruzado, A., Palanques, A., Arin, L., Gomis, D., Guillen, J., de Leon, A., Puigdefabregas, J., Sospedra,
766 J. and Velasquez, Z.R. (2002). Seasonal changes mass structure and shelf slope at the Ebre Shelf (NW
767 Mediterranean), *Continental Shelf Research* 22, 327–348.
- 768 Sánchez-Arcilla, A., González-Marco, D. and Bolaños, R. (2008) A review of wave climate and prediction along the Spanish
769 Mediterranean coast. *Natural Hazards Earth* 8, 1217–1228.
- 770 Sancho-García, A., Guillén, J. and Ojeda, E. (2013). Storm-induced readjustment of an embayed beach after modification by
771 protection works. *Geo-marine Letters* 33, 159-172.
- 772 Sherwood, C.R., Butman, B., Cacchione, D.A., Drake, D.E., Gross, T.F., Sternberg, R.W., Wiberg, P.L. and Williams III, A.J.
773 (1994). Sediment transport events of the northern California continental shelf during the 1990–1991 STRESS
774 experiments. *Continental Shelf Research* 14, 1063–1099.
- 775 Simarro, G., Guillén, J., Puig, P., Ribó, M., Lo Iacono, C., Palanques, A., Muñoz, A., Durán, R. and Acosta, J. (2015). Sediment
776 dynamics over sand ridges on a tideless mid-outer continental shelf. *Marine Geology* 361, 25–40.
- 777 Soulsby, R.L. (1997). *Dynamics of marine sands*. Thomas Telford Ltd., London, 249pp.
- 778 Soulsby, R.L. (2006). Simplified calculations of wave orbital velocities. TR-155. HR Wallingford Ltd., Wallingford, 12pp.
- 779 Spanish Port Authority. Puertos del Estado. Oceanografía y Meteorología. Banco de datos. Punto WANA 2066051.
780 <http://www.puertos.es/es-es/oceanografia/Portus/Paginas/Portus.aspx>. Last accessed: March 2016.
- 781 Traykovski, P., Geyer, W.R., Irish, J.D., and Lynch, J.F. (2000). The role of wave-induced density-driven fluid mud flows for
782 cross-shelf transport on the Eel River continental shelf. *Continental Shelf Research* 20, 2113–2140.
- 783 Ulses, C., Estournel, C., Durrieu de Madron, X., and Palanques, A. (2008). Suspended sediment transport in the Gulf of Lion
784 (NW Mediterranean): impact of extreme storms and floods, *Continental Shelf Research* 28, 2048–2070.
- 785 Urgelés, R., Cattaneo, A., Puig, P., Lique, C., De Mol, B., Amblàs, D., Sultan, N., and Trincardi, F. (2011). A review of
786 undulated sediment features on Mediterranean prodeltas: distinguishing sediment transport structures from sediment
787 deformation. *Mar Geophys Res* 32, 49–69.
- 788 Wiberg, P. and Smith, J.D. (1983). A comparison of field data and theoretical models for wave–current interactions at the bed on
789 the continental shelf. *Continental Shelf Research* 2, 147–162.
- 790 Wiberg, P.L., Drake, D.E. and Cacchione, D.A. (1994). Sediment resuspension and bed armoring during high bottom stress
791 events on the northern California continental shelf: measurements and predictions. *Continental Shelf Research* 14,
792 1191–1219.
- 793 Wiberg, P.L. and Sherwood, C.R. (2008). Calculating wave-generated bottom orbital velocities from surface-wave parameters.
794 *Computers & Geosciences* 34, 1243–1262.
- 795 WMO (1998). *Guide to wave analysis and forecasting*. World Meteorological Organization 702, Geneva, 159 pp.
- 796 Wright, L.D. (1995). *Morphodynamics of Inner Continental Shelves*. CRC Press, Boca Raton, 241pp.

Formatat: anglès (EUA)

Formatat: anglès (EUA)

Formatat: anglès (EUA)

Formatat: anglès (EUA)